ACS SENSORS

pubs.acs.org/acssensors Article

A Microfluidic Sensor for Continuous, In Situ Surface Charge Measurement of Single Cells

Liwei Ni, Rubia Shaik, Ruiting Xu, Ge Zhang,* and Jiang Zhe*

Cite This: https://dx.doi.org/10.1021/acssensors.9b02411 Read Online

ACCESS | Metrics & More | Article Recommendations | Supporting Information

ABSTRACT: Cell surface charge has been recognized as an important cellular property. We developed a microfluidic sensor based on resistive pulse sensing to assess surface charge and sizes of single cells suspended in a continuous flow. The device consists of two consecutive resistive pulse sensors (RPSs) with identical dimensions. Opposite electric fields were applied on the two RPSs. A charged cell in the RPSs was accelerated or decelerated by the electric fields and thus exhibited different transit times passing through the two RPSs. The cell surface charge is measured with zeta potential that can be quantified with the transit time difference. The transit time of each cell can be accurately detected with the width of pulses generated by the RPS, while the cell size can be calculated with the pulse magnitude at the same time. This device has the ability to detect surface charges and sizes of individual cells with high tolerance in cell types and testing solutions compared with traditional electrophoretic light scattering methods. Three different types of cells including HeLa cancer cells, human dermal fibroblast cells, and human umbilical vein endothelial cells (HUVECs) were tested with the sensor. Results showed a significant difference of zeta potentials between HeLa cells and fibroblasts or HUVECs. In addition, when HeLa cells were treated with various concentrations of glutamine, the effects on cancer cell surface charge were detected. Our results demonstrated the great potential of using our sensor for cell type sorting, cancer cell detection, and cell status analysis.

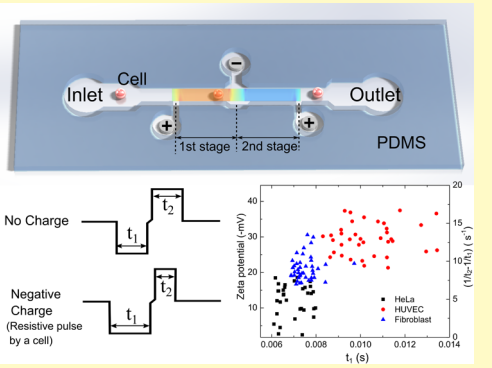

KEYWORDS: *surface charge, zeta potential, cell analysis, electrophoresis, resistive pulse sensing*

INTRODUCTION

Over past few decades, the advances in electrophysiology have revealed that cell surface charge is an important property of cell characteristics, which plays a crucial role in regulating cell functions.[1] Most cell surfaces are negatively charged and create a surface electrical potential that affecting ion concentrations at the cell membrane and consequently influencing important cellular events such as cell adhesion,[2] cellular uptake,[3] cell−cell communication, signal transduction, and protein trafficking.[4,5] Interestingly, recent studies reported that cell surface charge changes during different cell status and varies among cell types. For example, the cell surface charge of rat neural stem cells significantly altered during their differentiation process.[6] Negative surface charge increased during the maturation of human B lymphocytes.[7] Compared with normal cells, cancer cells generally have abnormal negative surface charge.[8−10] Therefore, the ability to rapidly measure the surface charge of individual cells will enable new approaches for cell detection and analysis.

To measure the cell surface charge, multiple methods have been developed, including electrostatic interaction, isoelectric equilibrium analysis, and electrophoresis. The electrostatic interaction method, usually based on the electrostatic interaction chromatography (ESIC) technique, uses charged ion-exchange resins/molecules to interact with cells; the affinity of the interaction depends on the cell surface charge.[11,12] Hence, from the affinity between cells and resins, relative cell surface charge can be evaluated. Recently, nanoprobes (NPs) with certain charges have also been used for cell surface charge detection in terms of measuring affinity between NPs and cells.[10] However, this type of methods does not provide direct surface charge measurement and is often time-consuming. For the isoelectric equilibrium analysis method, cells are loaded onto a column with a linear pH gradient and migrate under an appropriate voltage.[13] The cell surface charge can affect the isoelectric positions, which cells migrate to after isoelectric equilibrium. Although zeta potential of cells can be derived from the isoelectric positions, this method needs a long time to achieve isoelectric equilibrium. It is unsuitable for in situ measurement of single-cell surface charges. The electrophoresis method has been widely used for zeta potential measurement, which consists of microelectro-

Received: December 5, 2019
Accepted: January 15, 2020
Published: January 15, 2020

phoresis and electrophoretic light scattering. Microelectrophoresis applies a voltage across the cells suspended in the electrolyte and observes the movement of cells over a given distance.[14] The velocity of cells can be used to calculate electrophoretic mobility and zeta potential of cells. This method has proven to be effective in obtaining the zeta potential values of cells. Still, tracking individual cells over time is laborious and time-consuming.[11] More recent works have been using the electrophoretic light scattering method for zeta potential detection.[1,15] The velocity of cells under electric fields is measured in terms of the frequency change of the laser light scattered by the cell movement. However, using optical measurement for accurate capture of cell motions largely increases the complexity and cumbersomeness of operation. In addition, this method usually detects the motions of a group of cells suspended in a chamber, and the rapid movement of many cells makes the method hard to identify zeta potential for each single cell. Moreover to eliminate the numerous noise signals derived from the micro/nanoparticles (e.g., serum proteins, growth factors, and antibiotics) typically present in cell culture medium, specific testing solution (e.g. PBS) usually is required to suspend cells. Since the testing solution is not optimized for cell growth, potential cell status change and increased cell death may affect the accuracy of the measurement.

Recently, resistive pulse sensing has been used to determine zeta potentials of nano-objects.[16−20] This technique allows the particle-by-particle surface charge measurement by capturing the pulse signals when particles passing through a sensing channel or pore; the velocities/mobilities and therefore the zeta potentials of the particles can be calculated from the resistive pulses. This method allows measurements of both the size and zeta potential of each particle. It has been used to determine the zeta potential of emulsions,[21] liposomes,[22,23] and DNA-conjugated nanoparticles.[24−26] However, there are a few problems that need to be addressed. First, the resistive pulse sensing method relies on comparisons of transit times through the sensing channel with and without applying an electrophoretic electric field. Therefore, a reference test with exactly the same flow velocity without applying an electrophoretic electrical field must be conducted prior to the electrophoretic test. Second, in the reference test and electrophoretic test, while any difference in flow velocity would cause an error in cell velocity (and thus the zeta potential), fluid flow velocity must be accurately controlled, which increases the operation complexity. More importantly, in the reference and electrophoretic tests, the sequence of cells passing through the sensing channel could be different each time. As a result, identifying and comparing the resistive pulses induced by exactly the same cell in two separate experiments are impractical and difficult. While it works for particles with uniform surface charges and sizes, this approach is impractical for surface charge measurements of single cells in general due to the inhomogeneous nature of cells.

To overcome the above problems, we demonstrate a microfluidic device based on dual RPS stages to measure the zeta potential of single cells in situ without any reference test. The cells pass through two consecutive RPSs applied with opposite electric fields. By detecting the transit time difference through the two RPS stages, the zeta potential of each cell can be accurately measured, without a need to conduct any reference test. The zeta potential of each cell can be measured in situ in a continuous flow without a need for accurate flow control.

EXPERIMENTAL SECTION

Materials. The following materials were purchased from Sigma-Aldrich: HeLa cells, human negroid cervix epitheloid carcinoma-P9 (product# 93021013); minimum essential medium eagle, with ear (EMEM, product# M2279); L-glutamine solution Bioxtra, 200 mM (product# G7513); MEM nonessential amino acid, 100× (NEAA, product# M7145); fetal bovine serum (FBS, product# F0926); and 0.25% trypsin−EDTA solution (product# T4049), whereas Gibco DMEM high glucose 1× (product# 11995065), penicillin streptomycin (10,000 U/mL, product# 15140122), Dulbecco's phosphate-buffered salt solution 1× (DPBS, product# MT21031CV), and trypan blue solution 0.4% (product# SV3008401) were purchased from Thermo Fisher Scientific, and EGMTM-2 endothelial cell growth medium-2 BulletKit (product# CC-3162) was purchased from Lonza.

Sensing Principle. To detect the surface charge of single cells in situ in a continuous flow, we designed a microfluidic sensor, as shown in Figure 1. The sensor consisted of two successive resistive pulse sensors (RPSs), three Ag/AgCl electrodes I, II, and III placed in separate access holes, one inlet reservoir, and one outlet reservoir. An electric bridge circuit was used to apply the electric fields and measure the resistance changes of the two RPSs, shown in Figure 1b. R_1 and R_2 represent the resistance of the first and second RPSs. R_3 and R_4 are two external adjustable resistors used to (1) form a Wheatstone bridge with R_1 and R_2 and (2) maintain the electrophoretic voltage applied at electrodes I and III to be the same. A constant input voltage (V_{in}) is applied on the electric bridge circuit. When a cell passes through the two RPSs, it induces a small change in R_1 or R_2,[27] resulting in a small differential voltage between electrodes I and III. The differential voltage is amplified and detected as the output voltage (V_{out}). When a cell passes through the first RPS, R_1 increases, while R_2 remains unchanged; the output voltage drops accordingly. When the cell travels through the second RPS, R_2 increases, and the output voltage rises. Hence, when a cell passes the two successive RPSs, it generates one negative and one positive voltage pulses consecutively.

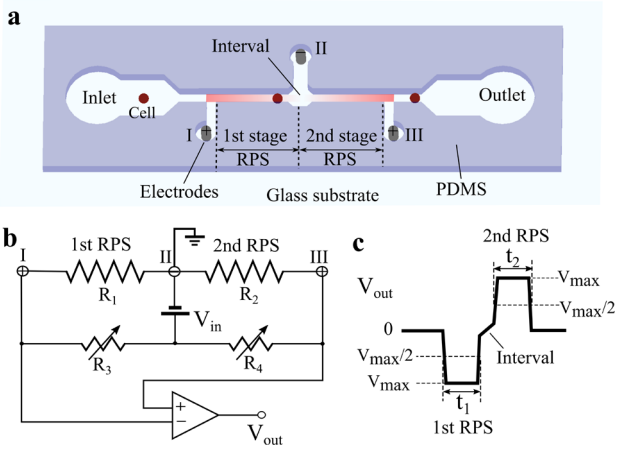

Figure 1. Schematic of the microfluidic sensor for in situ cell surface charge measurement. (a) Illustration of the two-stage resistive pulse sensing structures for cell surface charge measurement. (b) Scheme of the circuit for applying the electric field and measuring the resistive pulse. V_{in} = 10 V. The electrophoretic voltage V_e = 7.5 V. (c) Illustration of a typical resistive pulse signal when a cell passes the two-stage RPS consisting of a negative pulse and a positive pulse, separated by an interval with an alleviated slope.

The pulse width reflects the transit time/travel velocity through each RPS. Under an electric field, a charged cell experiences acceleration or deceleration due to electrophoretic motion, causing a change in transit time. Hence, the surface charge can be obtained

https://dx.doi.org/10.1021/acssensors.9b02411
ACS Sens. XXXX, XXX, XXX−XXX

from measuring the pulse width. Here, a small interval channel is designed between the two stages, which has a larger width than the RPS channel. There are two reasons to design this short interval channel: (1) to separate the two RPS stages because of the larger cross section, when a particle passes the interval channel, the change in channel resistance is reduced, causing a voltage change with an alleviated slope between the two resistive pulses (see Figure 1c), and (2) to reduce the transition effect due to sudden polarity change of electrophoretic electrical fields, which may cause variation in cell's transit time. Finite element analysis on the electrical field in the sensing area was conducted, showing the electric field was considerably uniform within the two RPS channels. Details of the simulation are provided in the Supporting Information.

The net electrical charge (or the magnitude of the surface charge) of a particle can be quantified by the zeta potential.[28] Zeta potential is the electric potential in the interfacial double layer of a dispersed particle or droplet versus a point in the continuous phase away from the interface.[29] The relation of the zeta potential ζ and the effective charge density σ_{eff} can be described with the Gouy−Chapman equation[30]

$$\sigma_{\text{eff}} = \sqrt{8cN\varepsilon_r\varepsilon_0 k_B T}\sin h\left(\frac{e\zeta}{2k_B T}\right) \quad (1)$$

where c is the ion concentration, N is the Avogadro constant, ε_r is the relative dielectric permittivity of the solution, ε_0 is the vacuum permittivity, k_B is the Boltzmann constant, and T is the temperature.

In this article, we used zeta potential to represent the cell surface charge property. To detect the zeta potential of single cells, we applied opposite electric fields on the two RPS stages. In the first RPS, a positive voltage is applied across electrodes I and II; a negative charged cell is decelerated. On the contrary, in the second RPS, a positive voltage is applied across electrodes II and III; when a cell travels through the second RPS, it is accelerated. The two RPSs have the same length l. The transit times through the two RPS stages are used to calculate the zeta potential ζ with the electrophoretic mobility μ of cells via the Helmholtz−Smoluchowski equation[30,31]

$$\zeta = \frac{\mu\eta}{\varepsilon_r\varepsilon_0} \quad (2)$$

$$\mu \equiv \nu/E \quad (3)$$

where η is the viscosity of the aqueous solution, and ν is the drift velocity of the particle or cell under an electric field ($E = V_e/l$). Because the carrier flow velocities are the same in the two RPSs, the drift velocity can be calculated with the transit times t_1 and t_2 of cells crossing through the two RPS stages with the same length l

$$\mu = \frac{1}{E}\left(\frac{1}{t_2} - \frac{1}{t_1}\right) \times \frac{1}{2} = \frac{1}{2E}\left(\frac{1}{t_2} - \frac{1}{t_1}\right) \quad (4)$$

Thus, by capturing the transit times t_1 and t_2, the zeta potential ζ can be calculated

$$\zeta = \frac{\eta l}{2E\varepsilon_r\varepsilon_0}\left(\frac{1}{t_2} - \frac{1}{t_1}\right) \quad (5)$$

The sensor is designed to capture the transit times through the two RPS stages in situ in a continuous flow. Therefore, the zeta potential of single cells can be obtained contiguously one by one without any reference test. The particle/cell size can be calculated from the pulse magnitude.[32−34] The relation between the size and the pulse magnitude can be found in the Supporting Information.

A similar structure of two successive microchannels was used in our prior study[35] aiming to detect magnetic bead-labeled cells via travel velocity that was affected by a magnetic field. The major merits of the current structure are as follows: (1) the use of an interval channel reduces the transition effect and helps identify two successive resistive pulses; (2) cell's travel velocity is affected by the applied voltage, without a need for any external actuator; and (3) the measurement is label-free.

Device Fabrication. The standard soft lithography method was used to fabricate the microfluidic sensor, shown in Figure 2. First, an

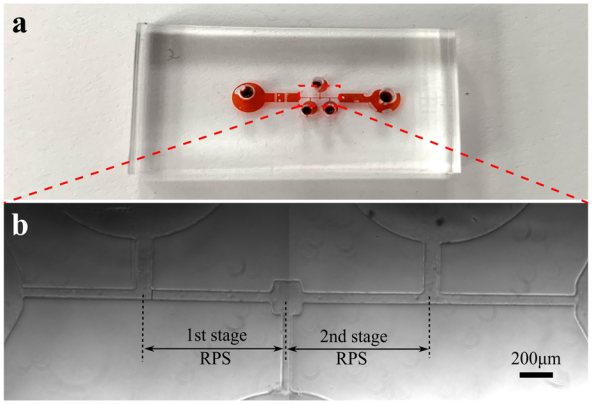

Figure 2. Pictures of the two-stage RPS sensor. (a) Picture of the microfluidic sensor on a glass substrate. (b) Microscopic image of the two RPS sensing channels and the interval channel.

SU-8 (2025, MicroChem, MA, USA) master pattern was created, consisting of the two RPS channels, an interval channel, three detecting arm channels where the electrodes are placed, one inlet reservoir, and one outlet reservoir. Next, a polydimethylsiloxane (PDMS) slab was made by pouring the PDMS on top of the SU-8 master to transfer the pattern, followed by degassing and curing the PDMS. Then, the inlet reservoir, electrode interface, and outlet reservoir were created by punching the PDMS slab with biopsy punches. Finally, the whole PDMS slab was bonded to a glass substrate after air plasma treatment (200 mTorr, 50 W, 50 s). The nominal dimensions of the two successive RPS channels are 60 μm (width), 45 μm (depth), and 700 μm (length) for both stages. The dimensions measured by the surface profilometer (Dektak 150, Veeco Instrument, NY, USA) were 58.08 ± 2.47 μm (width), 48.87 ± 2.74 μm (depth), and 711.87 ± 3.43 μm (length) for the first RPS and 55.82 ± 2.66 μm (width), 50.13 ± 2.31 μm (depth), and 718.16 ± 4.23 μm (length) for the second RPS. The interval between the first and second stages was 76.03 μm (length) and 189.97 μm (width). Three Ag/AgCl electrodes (1 mm in diameter) were inserted into the detecting arm channel to measure the resistive pulses from the two RPSs. The diameters of inlet and outlet holes were 1.5 mm.

Testing Procedures. For each test, the particle or single-cell suspension was loaded into the inlet reservoir and driven through the device by a constant pressure of 3 kPa from a flow controller (Flow-EZ, Fluigent, France). The pressure and flow rate were chosen to achieve the suitable pulse width. While at a high flow rate, the cell counting rate can be improved, and the resistive pulses may be too narrow. It is difficult to capture the complete shapes of narrow resistive pulses and thus identify the pulse width difference between the two successive resistive pulses, leading to lower resolution for the zeta potential measurement. A high pressure might also cause leakage between the PDMS channel and the glass substrate. A cell concentration of 100 cells/μL was used for the experiments. A direct current voltage of 10 V was applied on the electric bridge circuit (V_{in}). By adjusting the R_3 and R_4 (in the range of 5 to 500 kΩ), electrophoretic voltages of 7.5 and −7.5 V were applied on the first and second stages of RPS. The electric field applied on each channel was estimated to be 10.7 V/mm. An external circuit was used to amplify the voltage output with an instrumentation amplifier (AD620BN, Analog Devices Inc., USA). The gain for the amplifier is 100. The amplified signal was recorded at a sampling rate of 500 kHz with an NI-DAQ board (PCI-6133, National Instruments, USA). The recorded voltage signals were analyzed using a custom MATLAB program. The particle and cell sizes can be calculated from the recorded pulse magnitude. The zeta potentials can be calculated from the transit time difference. All quantified results demonstrated in

https://dx.doi.org/10.1021/acssensors.9b02411
ACS Sens. XXXX, XXX, XXX−XXX

means ± standard deviation were obtained from more than 100 independent values. Further increasing the data points did not cause a significant change in the results. Student's t test was conducted to compare significant differences between experimental groups. A p value of less than 0.05 was considered as statistically significant.

Because the width and the depth of the sensing channel were approximately two times of the tested sizes of cells/particles, there should be a gap in the micrometer level when the particles and cells passed through the RPSs. Because (1) the gap was much larger than the double layer thickness of the channel walls and (2) the electroosmotic flow is weak due to low voltage, the surface charge of the walls was unlikely to affect the cells' motions and hence the zeta potential measurement.

Joule heating could be a problem when the electrical current is relatively large. In our device, the electrical current through the RPS channel was approximately 7.81 μA. Calculation showed that such a small current was unlikely to generate a significant temperature gradient affecting the cells' viability and movement during the measurement. In fact, in a prior study,[36] we used similar resistive pulse sensing for cell analysis with a higher electrical current (12.7 μA); good cell viability was observed after the tests.

Particles for Device Calibration. Three types of standard microparticles with different surface coatings were used to calibrate the device: yellow polyethylene microspheres (YPMS), black paramagnetic polyethylene microspheres (BKPMS), and fluorescent green (UV) polyethylene microspheres (UVPMS) (polyethylene microsphere, Cospheric, CA, USA). These particles were diluted in phosphate-buffered saline (PBS) with a concentration of 100 particles/μL. The sizes of three types of particles were measured with AccuSizer single particle optical sizing (SPOS) systems (LE400, Entegris, MA, USA). The zeta potentials of these particles were measured using Zetasizer (Nano Z, Malvern Panalytical, UK). Next, these particles with the known sizes and zeta potentials were loaded to the device for calibration purpose.

Cell Culture and Glutamine Treatment. After the calibration, cells were tested to demonstrate in situ surface charge measurement capability of the sensor. Three types of cells including HeLa cells, human umbilical vein endothelial cells (HUVECs), and human dermal fibroblast cells (HDFs) were tested using our device. Each cell was cultured in their own optimized growth medium supplemented with 1% penicillin. For HeLa cells, the growth medium was EMEM medium with 10% FBS, 1% NEAA, and 2 mM glutamine. The growth medium of HDFs was DMEM medium with 10% FBS. The complete EGM-2 medium was used as the growth medium for HUVECs. All three types of cells were cultured in a humidified environment at 37 °C with 5% CO_2. The growth medium was then replaced every day. For device testing, cells were harvested and resuspended in their growth media with a concentration of 100 cells/μL for surface charge measurement. To test the influence of glutamine concentration on the surface charge of HeLa cells, various concentrations of glutamine (2, 6, and 10 mM) were added to the growth medium of HeLa cells. After 48 h of treatment, cells were harvested and suspended in the growth medium at a concentration of 100 cells/μL for zeta potential measurement using our device.

RESULTS AND DISCUSSION

Resistive Pulses of the Two-Stage RPS. Three different types of particles, YPMS, UVPMS, and BKPMS, were loaded into the device separately in suspension flows. The resistive pulses of microparticles passing through the two RPSs are shown in Figure 3. A negative pulse and a positive pulse were observed consecutively when a particle passed through the first and second RPSs. There was an interval ramp with an alleviated slope between the negative and positive pulses, when the particle passed through the short interval channel between the first and second RPSs. The transit time through each RPS is defined as the full width at half-maximum (FWHM) of the resistive pulse (Figure 1c). The FWHM of a pulse is measured

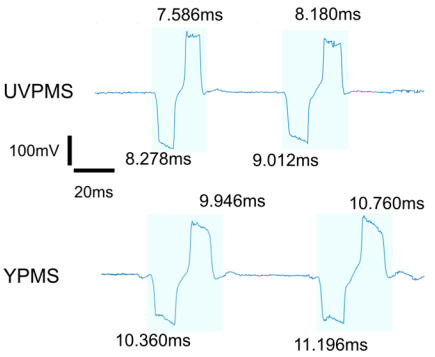

Figure 3. Typical resistive pulses of particles passing through the two RPSs. Significant difference in the transit time through the first and second RPSs was observed.

between the two points having half the maximum amplitude. Using FWHM as the transit time duration in this device can eliminate the entry effects of resistive pulse signals (i.e., a particle starts to induce a voltage pulse before it fully enters the RPS channel).[34] The significant difference between the transit time of the first and second RPSs was observed for both types of particles, shown in Figure 3. The difference of transit times can be used to calculate the zeta potential of each particle.

The sloped peak tops of the resistive pulses in Figure 3 are likely caused by the entry effects of RPS, the rotational motions and off-axis effects of the particles, the fabrication error of the channels, and the signal acquisition.[37] Note that the peak tops had been observed to be not flat in multiple studies utilizing resistive pulse sensing.[36−39]

Validation and Calibration of the Device. As a demonstration of the resistive pulse sensing, we first checked its size measurement. From the voltage pulse magnitude, the particle sizes of YPMS, UVPMS, and BKPMS were calculated to be 31.04 ± 4.01 μm, 30.83 ± 3.49 μm, and 31.58 ± 3.94 μm in diameter, respectively. Compared to the measurements from the AccuSizer particle optical sizing system, 30.31 ± 3.31 μm, 29.17 ± 3.81 μm, and 30.91 ± 4.15 μm for the three types of particles, the two sets of measurement were in good agreement, which indicated the validity of the RPS. The measured size distribution is shown in Figure S2a−c in the Supporting Information.

Next, we calibrated the device for single-cell surface charge measurement using the three particles (YPMS, UVPMS, and BKPMS), which have various zeta potentials due to their different surface coatings. They were first tested with the Zetasizer Nano Z system. The zeta potentials of YPMS, UVPMS, and BKPMS were −15.26 ± 0.83 mV, −22.36 ± 3.98 mV, and −47.3 ± 3.49 mV, respectively. Note that before the measurement, we used zeta potential transfer standard particles (DTS1235, Malvern Panalytical, UK) with the known zeta potentials provided by the vendor to confirm the validity of the instrument. The measured value (−38.4 ± 2.9 mV) was in agreement with the known value (−42 ± 4.2 mV). Then, each type of particles was loaded into our sensor separately under the same pressure. We recorded the voltage pulses generated from all particles for analysis. Typical voltage pulses are shown in Figure 3. When one particle passed through the two RPS stages, two resistive pulses with reverse polarity were generated. By comparing the pulse width of two consecutive pulses, it is obvious that for each negatively charged microparticle, the transit time through the first RPS (t_1) is

https://dx.doi.org/10.1021/acssensors.9b02411
ACS Sens. XXXX, XXX, XXX−XXX

longer than that through the second RPS (t_2) due to electrophoretic deceleration in the first stage and acceleration in the second stage. The difference in $1/t_1$ and $1/t_2$ ($1/t_2 - 1/t_1$) of YPMS, UVPMS, and BKPMS particles was 6.11 ± 1.25 s^{-1}, 10.29 ± 1.93 s^{-1}, and 20.84 ± 3.47 s^{-1}, respectively, shown in Figure 4. The results showed that the ($1/t_2 - 1/t_1$) value

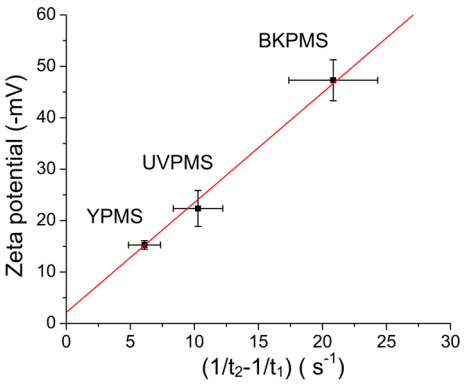

Figure 4. ($1/t_2 - 1/t_1$) measured from microparticles of YPMS, UVPMS, and BKPMS with different zeta potentials.

was nearly proportional to the zeta potential values of particles, which can be explained by eq 5. The linear fitting line is shown in Figure 4. The correlation between the transit time difference and the zeta potential is obtained

$$\zeta = 2.1381\left(\frac{1}{t_2} - \frac{1}{t_1}\right) + 1.7509 \quad (6)$$

Equation 6 can be used as the calibration curve of particle's zeta potential versus ($1/t_2 - 1/t_1$). Note that the nonzero intercepts in eq 6 were mainly caused by the variation in the zeta potentials of the microparticles used for the calibration (see the vertical error bars in Figure 4). The factors contributing to the nonzero intercept include (1) the dimensions of the first and second RPSs have a small difference because of the fabrication error, and (2) due to the sudden change of electrophoretic field, a cell may not achieve electrophoresis force-flow drag force equilibrium, causing variation in transit time. The differences in channel width, depth, and length between RPS 1 and RPS 2 could certainly cause a difference in the pulse width, which can in turn induce an error in zeta potential if we directly use eq 5 to calculate the zeta potential. However, when we calibrated the relation between the zeta potential and ($1/t_2 - 1/t_1$), shown in Figure 4, the dimension difference from the microfabrication can be compensated by the calibration.

In theory, the zeta potential of a particle can be calculated from eq 5 without any calibration. However, to use eq 5, the viscosity and relative permittivity need to be precisely determined. While different cells may have different media, it is a challenge to measure these two parameters in situ, in particular for field applications. More importantly, it is difficult to determine the lengths of the first stage and second stage of RPS because of the entry effect, that is, a particle starts to induce a resistance/voltage change before it enters the RPS channel. Similarly, there is still a resistance/voltage change when the particle exits the RPS sensing channel. While the use of FWHM pulse width can reduce error in t_1 and t_2 caused by the transition, the exact lengths of the RPSs corresponding to the t_1 and t_2 are still difficult to determine. Hence, a calibration is still needed to overcome these challenges.

Identifying Cell Species via Measuring Zeta Potentials. With the calibration of eq 6, next, we used the device to

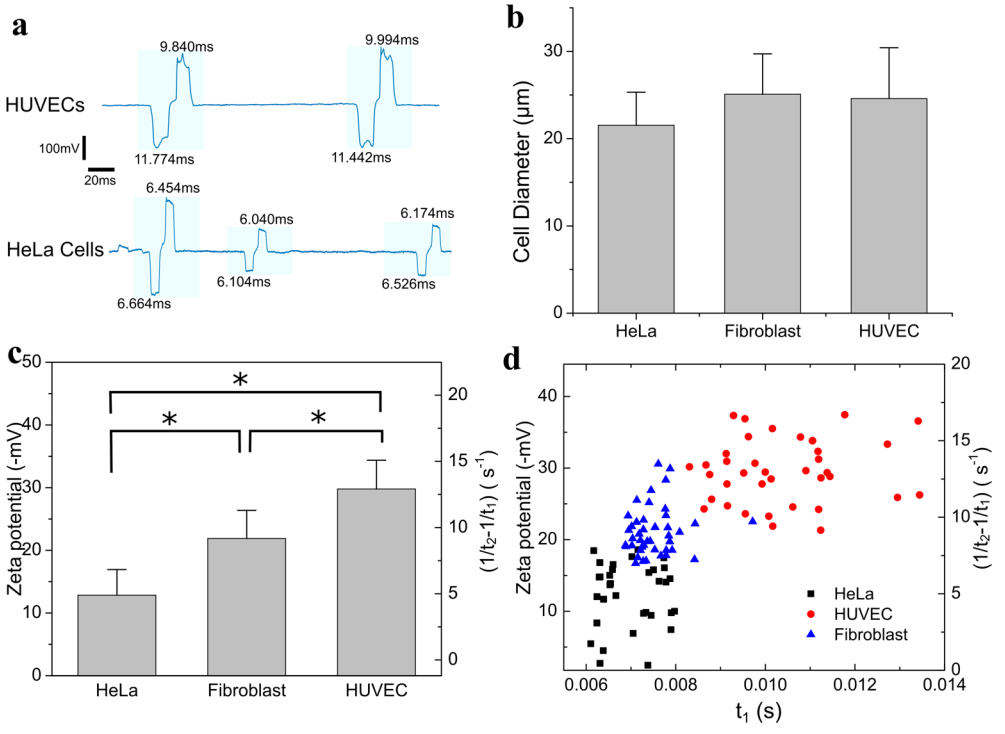

Figure 5. Resistive pulse sensing of HeLa cells, human dermal fibroblast cells (HDF), and HUVECs. (a) Typical pulses of HUVECs and HeLa cells. (b) Size measurement of the cells. (c) Measured ($1/t_2 - 1/t_1$) values for the three types of cells. (d) ($1/t_2 - 1/t_1$) and corresponded zeta potential versus t_1 for different cells. The asterisk symbol represents a statistically significant difference between two groups with p less than 0.05.

https://dx.doi.org/10.1021/acssensors.9b02411
ACS Sens. XXXX, XXX, XXX−XXX

measure the zeta potentials of HUVECs, fibroblast cells, and HeLa cells. These three types of cells represent three different types of properties and functions in human body. HUVECs are cells derived from the endothelium of veins and are widely used for the study of the function and pathology of endothelial cells. Fibroblast cells synthesize the extracellular matrix and collagen, produce the structural framework (stroma) for animal tissues, and play a critical role in wound healing. HeLa cells are cervical cancer cells used extensively as sample cells for cancer cells' functions and properties. Cell suspensions were introduced into the device separately. The magnitude and transit time of resistive pulses generating from each cell passing through the two RPSs were recorded to measure the size and zeta potential of single cells. Typical pulses generated by HUVECs and HeLa cells are given in Figure 5a. The equivalent diameter of the cells can be calculated from the pulse magnitude. The measured sizes of HeLa cancer cells, fibroblast cells, and HUVECs were 21.53 ± 3.79 μm, 25.09 ± 4.62 μm, and 24.60 ± 5.83 μm in diameter, respectively, shown in Figure 5b. The size distribution of the cells is shown in Figure S2d−f in the Supporting Information.

The transit times t_1 and t_2 were measured from resistive pulses generated by cells passing through the two RPSs, and the values $(1/t_2 - 1/t_1)$ of the three types of cells are plotted in Figure 5c,d. The results from statistical analysis shown in Figure 5c indicated that there was a significant difference of the transit time difference value $(1/t_2 - 1/t_1)$ among HeLa cells, HUVECs, and fibroblast cells. The $(1/t_2 - 1/t_1)$ values of HeLa cells, fibroblast cells, and HUVECs were 4.38 ± 2.32 s^{-1}, 9.41 ± 2.10 s^{-1}, and 13.67 ± 2.39 s^{-1}, respectively. The smaller $(1/t_2 - 1/t_1)$ value of HeLa cells implied that HeLa cells had smaller surface charges. The calculated zeta potential of HeLa cells, fibroblast cells, and HUVECs were −11.11 ± 4.96 mV, −21.88 ± 4.49 mV, and −30.97 ± 5.11 mV, respectively.

Note that the significant difference in the surface charge between normal and transformed cancer cells has also been reported in multiple studies.[8,9] The surface charge of cells is mainly due to the outer envelope macromolecules containing the ionized phosphate, carboxylate, and amino functions, which are exposed to the extracellular environment.[40] The cell surface charge is usually assessed via the zeta potential, which is the electrical potential between the cell surface and the aqueous environment.[41] The cell-type-specific membrane structure and redistribution of ions at cell membrane interfaces during certain cell status can cause changes of cell surface charge.[8] As a result, the zeta potential of the cells, represented by the transit time difference value $(1/t_2 - 1/t_1)$, can be used as an important marker to identify different cells or track the changes of cell status. While our sensor can clearly identify the group patterns in zeta potentials of the three types of cells, we noticed that there is a difference between the measured values of HeLa cells and HUVECs by our sensor and the reported values by prior studies.[42,43] The difference could be caused by the use of different solutions during cell surface charge measurement. Unlike other measurements that require the use of specific solution (e.g., PBS) during testing to eliminate the noise signal, this sensor can specifically detect cells from other particles in the cell culture medium, which allows measuring the cell surface charge in cell growth medium. The growth medium could help maintain high cell viability and stable cell surface property of the tested cells.

While the transit time t_1 (reflects the velocity of a cell passing through the RPS) alone is also representative of the zeta potential/surface charge of a cell, it is difficult to use t_1 to quantitatively determine the zeta potential. This is because the velocity of cell is dependent not only on the electrophoretic motion but also on the carrier flow rate induced by the applied pressure, geometry of the microchannel, and the entry effect of RPS. The size, shape, and orientation of the cell certainly cause variations on the resistive pulse width at t_1.[44] Even if a reference test without electrophoretic motion can be conducted to focus to compensate the carrier flow velocity and obtain only the electrophoretic velocity of a cell because individual cells have different sizes and surface charges, it would be very difficult to pair the resistive pulses of the same cell in two separate tests. Additionally, any flow variation during the test would also cause an error in the measurement. In contrast, with the unique two successive RPSs, we use $1/t_2 - 1/t_1$ to calculate the zeta potential, which can nearly eliminate the effects of cell size, shape, and orientation, carrier flow velocity, and the flow fluctuation without a need to conduct a reference test. With a calibration, other factors such as channel geometries, the entry effect, and the transition effect due to the sudden change of electrophoretic fields can also be taken into account. Using eq 6, we can calculate the zeta potential of the cells from $(1/t_2 - 1/t_1)$ values. Clearly, the data points of three types of cells form three distinct clusters, showing that the value $(1/t_2 - 1/t_1)$ measured from this device can be used to identify HeLa cancer cells from HUVECs and fibroblast cells in a continuous flow.

The above tests demonstrated the ability of this device to measure the zeta potential of each individual cell in a continuous flow. While many studies utilized electrophoretic light scattering method to measure the average zeta potential of a group of cells, it is difficult to measure the zeta potential of each single cell. In many biomedical applications (such as cell sorting, detecting cancer cells from circulating blood, and identifying stem cells from tissue lysate), individual cells in a continuous flow need to be analyzed. This device has the capability of scanning single cells in a continuous flow, which enables high-throughput detection. In addition, its simple structure allows it to be easily integrated with other microfluidic analysis into a chip.

Glutamine Effects on HeLa Cell Surface Charge. To explore the potential biomedical application of our device, we tested the glutamine effect on HeLa cell surface charge using our sensor. Cancer cells fundamentally differ from normal cells by having a much higher rate of glutamine metabolism. Most recently, studies have revealed the correlation between the cell surface charge and metabolic patterns.[45,46] In this study, we treated HeLa cells with three different concentrations of glutamine to alter their glutamine metabolism rate and assess their effects on surface charge.

The $(1/t_2 - 1/t_1)$ values of HeLa cells cultured at concentrations of 2, 6, and 10 mM were 4.79 ± 1.70 s^{-1}, 10.44 ± 1.27 s^{-1}, and 17.25 ± 1.12 s^{-1}, respectively. The calculated zeta potentials of HeLa cells cultured at these three concentrations were −11.98 ± 3.63 mV, −24.07 ± 2.73 mV, and −38.64 ± 2.39 mV, shown in Figure 6. The results showed that when increasing the glutamine concentration during the HeLa cell culturing process, the negative surface charge amount on the cell surface increased accordingly. Our results confirmed the similar observations from previous published studies[47] and proved the effects of glutamine on cancer cell surface charge.

https://dx.doi.org/10.1021/acssensors.9b02411
ACS Sens. XXXX, XXX, XXX−XXX

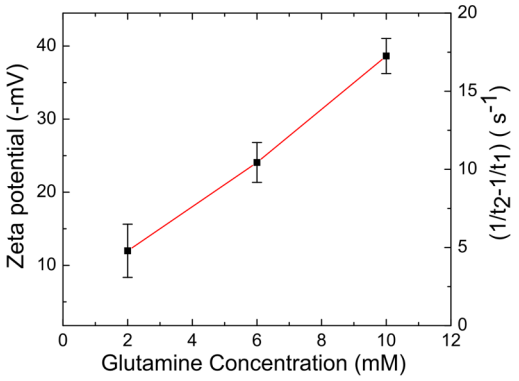

Figure 6. Measured $(1/t_2 - 1/t_1)$ and the calculated zeta potential of HeLa cells cultured under multiple glutamine concentrations.

Since this phenomenon is unique for cancer cells, it has the potential to be utilized as a highly sensitive biomarker for cancer cell detection. We envision in the future study that this sensor can be applied to capture the significant change of cell surface charge of individual cancer cells after glutamine treatment and use the identified change to not only detect cancer cells but also derive glutamine metabolic patterns for different cancer types.

CONCLUSIONS

We developed a microfluidic sensor that can measure zeta potentials of single cells in a cell growth medium. The device utilizes two successive resistive pulse sensors. By applying electrophoretic voltages on the two stages with reverse polarities, each charged cell exhibits different transit times when it passes through the two successive microresistive pulse sensing structures. The transit times are measured via the two successive voltage pulses generated by the cell. From the transit time difference, the electrophoretic mobility and thus the zeta potential of single cells can be obtained. The device can measure not only the zeta potential of each single cell in situ but also its size simultaneously without a need for a reference test or flow control. We validated and calibrated the device using three types of standard microparticles, YPMS, UVPMS, and BKPMS, which have different zeta potential values due to their surface coating. We then demonstrated that this device can identify different types of cells, such as HUVECs, fibroblast cells, and HeLa cells, versus their zeta potentials without labeling the cells. Further, we showed that the device can detect the surface charge change of HeLa cells when increasing the glutamine concentration during the culturing process. Results showed that this device has great potentials for cell type sorting, cancer cell identification, and cell status analysis.

ASSOCIATED CONTENT

Supporting Information

The Supporting Information is available free of charge at https://pubs.acs.org/doi/10.1021/acssensors.9b02411.

Supporting figures of electric field modeling and particle/cell size distribution (PDF)

AUTHOR INFORMATION

Corresponding Authors

Ge Zhang − *Department of Biomedical Engineering, University of Akron, Akron, Ohio 44325, United States*; Email: ge10@uakron.edu

Jiang Zhe − *Department of Mechanical Engineering, University of Akron, Akron, Ohio 44325, United States*; Email: jzhe@uakron.edu

Authors

Liwei Ni − *Department of Mechanical Engineering, University of Akron, Akron, Ohio 44325, United States*

Rubia Shaik − *Department of Biomedical Engineering, University of Akron, Akron, Ohio 44325, United States*

Ruiting Xu − *Department of Mechanical Engineering, University of Akron, Akron, Ohio 44325, United States*

Complete contact information is available at: https://pubs.acs.org/10.1021/acssensors.9b02411

Notes

The authors declare no competing financial interest.

ACKNOWLEDGMENTS

This work was supported by the National Science Foundation of USA under award numbers ECCS 1625544, ECCS 1905786, and DBI 1911526.

REFERENCES

(1) Wilson, W. W.; Wade, M. M.; Holman, S. C.; Champlin, F. R. Status of Methods for Assessing Bacterial Cell Surface Charge Properties Based on Zeta Potential Measurements. *J. Microbiol. Methods* **2001**, *43*, 153−164.

(2) Metwally, S.; Stachewicz, U. Surface Potential and Charges Impact on Cell Responses on Biomaterials Interfaces for Medical Applications. *Mater. Sci. Eng. C* **2019**, *104*, 109883.

(3) Fröhlich, E. The Role of Surface Charge in Cellular Uptake and Cytotoxicity of Medical Nanoparticles. *Int. J. Nanomed.* **2012**, *7*, 5577−5591.

(4) Tsai, C. C.; Hung, H. H.; Liu, C. P.; Chen, Y. T.; Pan, C. Y. Changes in Plasma Membrane Surface Potential of PC12 Cells as Measured by Kelvin Probe Force Microscopy. *PLoS One* **2012**, *7*, No. e33849.

(5) Goldenberg, N. M.; Steinberg, B. E. Surface Charge: A Key Determinant of Protein Localization and Function. *Cancer Res.* **2010**, *70*, 1277−1280.

(6) Chou, Y. S.; Lu, J. N.; Li, Y. C.; Wang, J. H.; Young, T. H. The Surface Potential Variation of Neural Stem/Progenitor Cells during Differentiation Process. *J. Neurol. Neurosci.* **2015**, *06*, 1−8.

(7) Bauer, J.; Kachel, V.; Hannig, K. The Negative Surface Charge Density Is a Maturation Marker of Human B Lymphocytes. *Cell. Immunol.* **1988**, *111*, 354−364.

(8) Cook, G. M. W.; Jacobson, W. The Electrophoretic Mobility of Normal and Leukaemic Cells of Mice. *Biochem. J.* **1968**, *107*, 549−557.

(9) Zhang, Y.; Yang, M.; Portney, N. G.; Cui, D.; Budak, G.; Ozbay, E.; Ozkan, M.; Ozkan, C. S. Zeta Potential: A Surface Electrical Characteristic to Probe the Interaction of Nanoparticles with Normal and Cancer Human Breast Epithelial Cells. *Biomed. Microdevices* **2008**, *10*, 321−328.

(10) Shi, D. Cancer Cell Surface Negative Charges: A Bio-Physical Manifestation of the Warburg Effect. *Nano Life* **2017**, *07*, 1771001.

(11) Pedersen, K. Electrostatic Interaction Chromatography, a Method for Assaying the Relative Surface Charges of Bacteria. *FEMS Microbiol. Lett.* **1981**, *12*, 365−367.

(12) Dickson, J. S.; Koohmaraie, M. Cell Surface Charge Characteristics and Their Relationship to Bacterial Attachment to Meat Surfaces. *Appl. Environ. Microbiol.* **1989**, *55*, 832−836.
(13) Sherbet, G. V.; Lakshmi, M. S. Characterisation of Escherichia Coli Cell Surface by Isoelectric Equilibrium Analysis. *Biochim. Biophys. Acta, Biomembr.* **1973**, *298*, 50−58.
(14) Bier, M. *Electrophoresis: Theory, Methods, and Applications*; Elsevier, 2013.
(15) Blake, R. C., II; Shute, E. A.; Howard, G. T. Solubilization of Minerals by Bacteria: Electrophoretic Mobility of Thiobacillus Ferrooxidans in the Presence of Iron, Pyrite, and Sulfur. *Appl. Environ. Microbiol.* **1994**, *60*, 3349−3357.
(16) Sikora, A.; Shard, A. G.; Minelli, C. Size and ζ-Potential Measurement of Silica Nanoparticles in Serum Using Tunable Resistive Pulse Sensing. *Langmuir* **2016**, *32*, 2216−2224.
(17) Vogel, R.; Anderson, W.; Eldridge, J.; Glossop, B.; Willmott, G. A Variable Pressure Method for Characterizing Nanoparticle Surface Charge Using Pore Sensors. *Anal. Chem.* **2012**, *84*, 3125−3131.
(18) Ito, T.; Sun, L.; Crooks, R. M. Simultaneous Determination of the Size and Surface Charge of Individual Nanoparticles Using a Carbon Nanotube-Based Coulter Counter. *Anal. Chem.* **2003**, *75*, 2399−2406.
(19) Blundell, E. L. C. J.; Vogel, R.; Platt, M. Particle-by-Particle Charge Analysis of DNA-Modified Nanoparticles Using Tunable Resistive Pulse Sensing. *Langmuir* **2016**, *32*, 1082−1090.
(20) Arjmandi, N.; Van Roy, W.; Lagae, L.; Borghs, G. Measuring the Electric Charge and Zeta Potential of Nanometer-Sized Objects Using Pyramidal-Shaped Nanopores. *Anal. Chem.* **2012**, *84*, 8490−8496.
(21) Somerville, J. A.; Willmott, G. R.; Eldridge, J.; Griffiths, M.; McGrath, K. M. Size and Charge Characterisation of a Submicrometre Oil-in-Water Emulsion Using Resistive Pulse Sensing with Tunable Pores. *J. Colloid Interface Sci.* **2013**, *394*, 243−251.
(22) Kozak, D.; Broom, M.; Vogel, R. High Resolution Particle Characterization to Expedite Development and Regulatory Acceptance of Nanomedicines. *Curr. Drug Delivery* **2015**, *12*, 115−120.
(23) Maas, S. L. N.; De Vrij, J.; Van Der Vlist, E. J.; Geragousian, B.; Van Bloois, L.; Mastrobattista, E.; Schiffelers, R. M.; Wauben, M. H. M.; Broekman, M. L. D.; Nolte-'T Hoen, E. N. M. Possibilities and Limitations of Current Technologies for Quantification of Biological Extracellular Vesicles and Synthetic Mimics. *J. Controlled Release* **2015**, *200*, 87−96.
(24) Adela Booth, M.; Vogel, R.; Curran, J. M.; Harbison, S. A.; Travas-Sejdic, J. Detection of Target-Probe Oligonucleotide Hybridization Using Synthetic Nanopore Resistive Pulse Sensing. *Biosens. Bioelectron.* **2013**, *45*, 136−140.
(25) Healey, M. J.; Rowe, W.; Siati, S.; Sivakumaran, M.; Platt, M. Rapid Assessment of Site Specific DNA Methylation through Resistive Pulse Sensing. *ACS Sens.* **2018**, *3*, 655−660.
(26) Mayne, L.; Lin, C. Y.; Christie, S. D. R.; Siwy, Z. S.; Platt, M. The Design and Characterization of Multifunctional Aptamer Nanopore Sensors. *ACS Nano* **2018**, *12*, 4844−4852.
(27) Liu, F.; KC, P.; Zhang, G.; Zhe, J. A Microfluidics Based Magnetic Beads Assay For Label Free Cell Analysis. In *2015 Annual Meeting of the Biomedical Engineering Society*, Tampa, Florida, Oct. 8th; 2015.
(28) Dukhin, A. S.; Goetz, P. J. Fundamentals of Interface and Colloid Science. In *Characterization of Liquids, Nano- and Microparticulates, and Porous Bodies Using Ultrasound*; 2010, pp 21−89, DOI: 10.1016/S1383-7303(10)23002-8.
(29) Lu, G. W.; Gao, P. Emulsions and Microemulsions for Topical and Transdermal Drug Delivery. In *Handbook of Non-Invasive Drug Delivery Systems*; 2010, pp 59−94, DOI: 10.1016/b978-0-8155-2025-2.10003-4.
(30) Ge, Z.; Wang, Y. Estimation of Nanodiamond Surface Charge Density from Zeta Potential and Molecular Dynamics Simulations. *J. Phys. Chem. B* **2016**, *121*, 3394−3402.
(31) Hunter, R. J. *Zeta Potential in Colloid Science - Principles and Applications*; Ottewill, R. H.; Rowell, R. L., Eds.; Elsevier, 1981.
(32) Carbonaro, A.; Sohn, L. L. A Resistive-Pulse Sensor Chip for Multianalyte Immunoassays. *Lab Chip* **2005**, *5*, 1155−1160.
(33) Jagtiani, A. V.; Carletta, J.; Zhe, J. A Microfluidic Multichannel Resistive Pulse Sensor Using Frequency Division Multiplexing for High Throughput Counting of Micro Particles. *J. Micromech. Microeng.* **2011**, *21*, No. 065004.
(34) DeBlois, R. W.; Bean, C. P. Counting and Sizing of Submicron Particles by the Resistive Pulse Technique. *Rev. Sci. Instrum.* **1970**, *41*, 909−916.
(35) Liu, F.; KC, P.; Zhang, G.; Zhe, J. In Situ Single Cell Detection via Microfluidic Magnetic Bead Assay. *PLoS One* **2017**, *12*, No. e0172697.
(36) Liu, F.; KC, P.; Zhang, G.; Zhe, J. Microfluidic Magnetic Bead Assay for Cell Detection. *Anal. Chem.* **2015**, *88*, 711−717.
(37) Kozak, D.; Anderson, W.; Vogel, R.; Trau, M. Advances in Resistive Pulse Sensors: Devices Bridging the Void between Molecular and Microscopic Detection. *Nano Today* **2011**, *6*, 531−545.
(38) Saleh, O. A.; Sohn, L. L. Quantitative Sensing of Nanoscale Colloids Using a Microchip Coulter Counter. *Rev. Sci. Instrum.* **2001**, *72*, 4449−4451.
(39) Willmott, G. R.; Parry, B. E. T. Resistive Pulse Asymmetry for Nanospheres Passing through Tunable Submicron Pores. *J. Appl. Phys.* **2011**, *109*, No. 094307.
(40) Mozes, N.; Léonard, A. J.; Rouxhet, P. G. On the Relations between the Elemental Surface Composition of Yeasts and Bacteria and Their Charge and Hydrophobicity. *Biochim. Biophys. Acta, Biomembr.* **1988**, *945*, 324−334.
(41) Saito, T.; Takatsuka, T.; Kato, T.; Ishihara, K.; Okuda, K. Adherence of Oral Streptococci to an Immobilized Antimicrobial Agent. *Arch. Oral Biol.* **1997**, *42*, 539−545.
(42) Hondroulis, E.; Zhang, R.; Zhang, C.; Chen, C.; Ino, K.; Matsue, T.; Li, C. Z. Immuno Nanoparticles Integrated Electrical Control of Targeted Cancer Cell Development Using Whole Cell Bioelectronic Device. *Theranostics* **2014**, *4*, 919.
(43) Selvi, R. B.; Chatterjee, S.; Jagadeesan, D.; Chaturbedy, P.; Suma, B. S.; Eswaramoorthy, M.; Kundu, T. K. ATP Driven Clathrin Dependent Entry of Carbon Nanospheres Prefer Cells with Glucose Receptors. *J. Nanobiotechnol.* **2012**, *10*, 35.
(44) Maugi, R.; Hauer, P.; Bowen, J.; Ashman, E.; Hunsicker, E.; Platt, M. A methodology for characterising nanoparticle size and shape using nanopores. *Nanoscale* **2020**, *12*, 262−270.
(45) Le, W.; Chen, B.; Cui, Z.; Liu, Z.; Shi, D. Detection of Cancer Cells Based on Glycolytic-Regulated Surface Electrical Charges. *Biophys. Rep.* **2019**, *5*, 10−18.
(46) Wang, Y.; Han, X.; Cui, Z.; Shi, D. Bioelectricity, Its Fundamentals, Characterization Methodology, and Applications in Nano-Bioprobing and Cancer Diagnosis. *Adv. Biosyst.* **2019**, *3*, 1900101.
(47) Chen, B.; Le, W.; Wang, Y.; Li, Z.; Wang, D.; Ren, L.; Lin, L.; Cui, S.; Hu, J. J.; Hu, Y.; Yang, P.; et al. Targeting Negative Surface Charges of Cancer Cells by Multifunctional Nanoprobes. *Theranostics* **2016**, *6*, 1887−1898.

https://dx.doi.org/10.1021/acssensors.9b02411
ACS Sens. XXXX, XXX, XXX−XXX